Open access • Journal Article • DOI:10.3390/APP11146304

Laser Synthesized Graphene and Its Applications — Source link

Vittorio Scardaci

Published on: 08 Jul 2021 - Applied Sciences (Multidisciplinary Digital Publishing Institute)

Topics: Graphene

applied sciences

MDPI

Review

Laser Synthesized Graphene and Its Applications

Vittorio Scardaci

Dipartimento di Scienze Chimiche, Università degli Studi di Catania, Viale Andrea Doria 6, 95125 Catania, Italy; vittorio.scardaci@unict.it

Abstract: Since graphene was discovered, a great deal of research effort has been devoted to finding more and more effective synthetic routes, stimulated by its astounding properties and manifold promising applications. Over the past decade, laser synthesis has been proposed as a viable synthesis method to reduce graphene oxide to graphene as well as to obtain graphene from other carbonaceous sources such as polymers or other natural materials. This review first proposes to discuss the various conditions under which graphene is obtained from the reduction of graphene oxide or is induced from other materials using laser sources. After that, a wide range of applications proposed for the obtained materials are discussed. Finally, conclusions are drawn and the author's perspectives are given.

Keywords: graphene; laser; graphene oxide; polymers; natural sources; sensing; energy storage; wearables; environmental; antimicrobial

Citation: Scardaci, V. Laser Synthesized Graphene and Its Applications. *Appl. Sci.* **2021**, *11*, 6304. https://doi.org/10.3390/app11146304

Academic Editors: Petr Korusenko and Sergey Nesov

Received: 6 June 2021
Accepted: 1 July 2021
Published: 8 July 2021

1. Introduction

The outstanding properties that graphene has demonstrated since its discovery have sparked a huge research and development effort across multiple fields, including but not limited to electronics, optics, materials science, sensing, biology, medicine, photonics, just to name a few. Such efforts have been devoted not only to exploring and understanding the properties, but also to finding new ways to synthesize, process, and deposit graphene to fit new applications. Indeed, a range of methods has been proposed, with pros and cons that make each method suitable for specific types of applications. The method that led to the discovery of graphene, mechanical exfoliation, while producing excellent pristine graphene flakes, is generally only suitable for lab-scale testing of graphene's fundamental properties [1–3]. Chemical vapor deposition (CVD) is able to produce large area graphene layers on a substrate, which can be patterned or transferred, and are suitable for optics or electronics applications [4–7], but this method is limited if large quantities of material are needed for further processing. Liquid phase exfoliation, on the other hand, is able to produce large quantities of graphene flakes in organic solvents or in water with the aid of surfactants or polymers [8–11]. This method has wide flexibility in terms of further processing and applications, although flakes are small if compared to those obtained by CVD.

Oxidation of graphite is a method for dispersing graphene layers in aqueous solution with no other aid [12]. This method, however, involves the introduction of oxygen-containing functional groups, such as –OH, –COOH, or epoxy, which significantly alter the structure of graphene and thus its properties [13,14]. This material is known as graphene oxide (GO). While some applications can benefit from GO with no further processing, other applications require GO to be reduced to reestablish the original graphene properties after the material has been processed [15]. This can be typically achieved by chemical reduction [16,17], and the material is commonly referred to as reduced GO (rGO), to distinguish it from pristine graphene as it still contains residual functional groups.

Laser synthesis (LS) has been brought up over the last decade as an easy, fast, and cheap alternative method for the production of graphene. This method can achieve an

effective reduction of GO as this is deposited onto a surface [14,18,19]. This type of rGO is commonly referred to as laser-reduced graphene (LRG). Laser synthesis was also applied on non-graphitic sources such as polymers or other natural materials, on which the action of the laser can induce a transformation into graphene [20–23]. In this case, the material obtained is referred to as laser-induced graphene (LIG). Beyond providing an easy graphene synthesis method, via GO reduction or modification of other materials, LS has the intrinsic potential to create graphene patterns without using costly lithographic methods [24–26] at the resolution of the laser beam, i.e., down to 1 µm, making it very appealing for a wide range of applications.

While many other reviews have appeared on this topic (see for example Refs. [27–31]), most focus on a selected range of applications or sources. This paper, on the other hand, aims at reviewing synthesis methods of both LRG and LIG, their characterization, and a full spectrum of applications. Section 2 briefly discusses the fundamentals of LS, the different sources, conditions and types of laser methods, as well as the characterization of the materials. Section 3 covers the applications that have been proposed over the years for both LRG and LIG, while Section 4 provides perspectives and conclusions.

2. Laser Synthesis of Graphene

Before the laser reduction of GO was first reported, the use of a Xenon flash lamp was proposed for GO reduction by Cote et al. in 2009 [32]. The authors observed the loss of oxygen-containing groups by Fourier-transform infrared (FTIR) spectroscopy. A similar approach was reported by Choi et al. [33], who used a Xenon flash lamp to induce GO reduction onto a polyimide (PI) substrate. This study indeed showed through X-ray photoelectron spectroscopy (XPS) that O-containing bonds were lost during the process; however, the reported Raman spectra did not support the formation of graphene monolayers. Nevertheless, the material was used for gas sensing applications, which will be discussed in the next section. The first report of a laser reduction of graphene appeared in 2010 [18]. Here, the authors produced LRG patterns from GO coated onto a substrate using a femtosecond laser at 790 nm wavelength that was programmed for a raster movement (Figure 1a), thus reducing and patterning GO at the same time, with resolution down to a few micrometers. By XPS it was observed that the signal from C-O bonds was significantly reduced in laser-treated areas, while C-C signal was intact (Figure 1b) [18]. Later, Trusovas et al. [34] investigated the formation of LRG as a function of the energy transferred by a picosecond laser. Using Raman spectroscopy, and evaluating the width of the characteristic spectral features (G- D- and 2D-bands), they determined that order in the material was increased by increasing laser irradiation and dose (Figure 2).

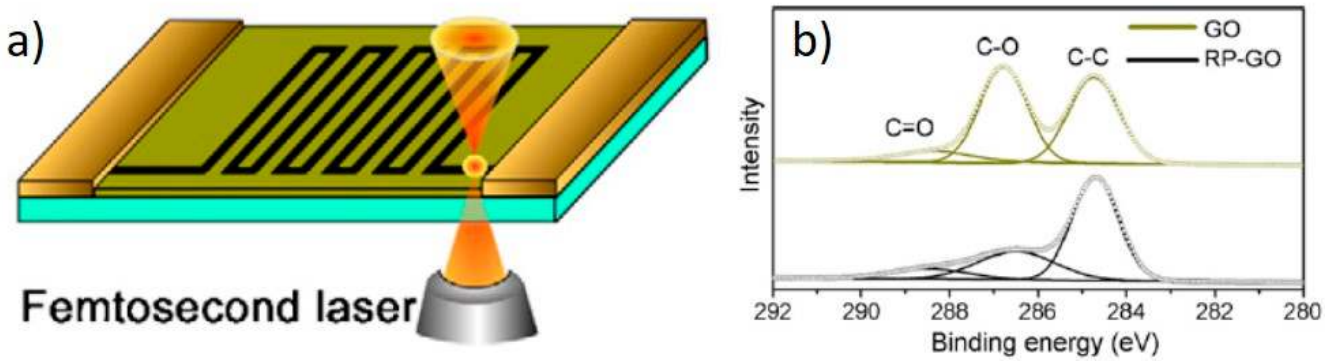

Figure 1. (**a**) Schematics of the LS process, with simultaneous GO reduction and patterning (RP). (**b**) XPS data from GO and reduced and patterned (RP) GO. Reproduced with permission from Ref. [18]. Copyright 2010, Elsevier.

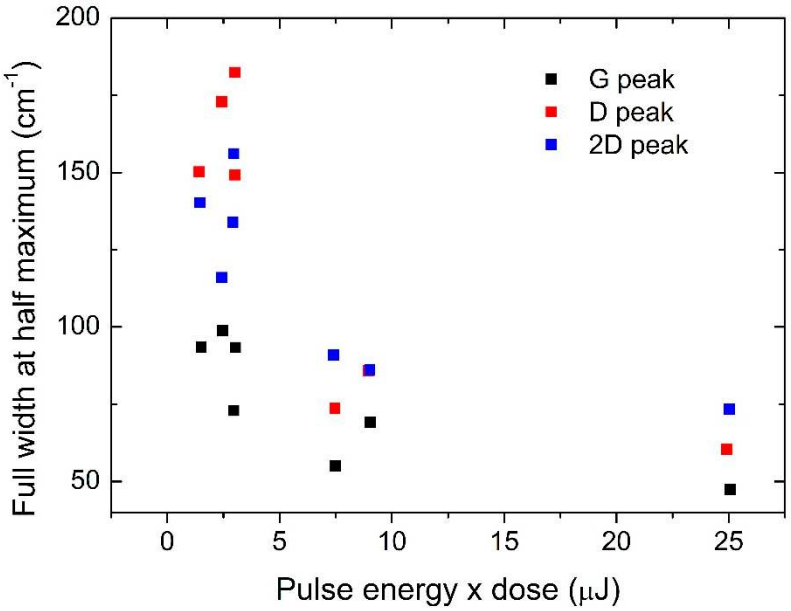

Figure 2. Raman parameters as function of laser irradiation. Reproduced with permission from Ref. [34]. Copyright 2013, Elsevier.

Only a few years later, the production of LRG was demonstrated using the laser from a DVD source with a simple commercially available LightScribe software [19,35,36]. Here, the process was again quite simple, as a GO solution was drop-cast onto a flexible substrate, shaped like a DVD disc, then dried and exposed to the DVD laser. It was clearly observed that the exposed area was significantly modified, as XPS spectra showed that O-containing bonds almost disappeared and the Raman spectrum was modified to confirm the formation of graphene [35]. Electron microscopy also showed that the exposed area was swollen as layers that were initially well-stacked then appeared as exfoliated.

The effect of the type of laser for LS was studied by Arul et al. [37], who investigated a femtosecond laser (100 fs pulse, 800 nm wavelength), a nanosecond laser (10 ns, 248 nm), and a continuous laser (LightScribe, 788 nm). It was found that the most effective laser process is with the nanosecond laser, since they observed both oxygen loss and graphenization, while by femtosecond laser the authors observed oxygen removal but no graphenization. By continuous laser irradiation, oxygen was removed but defects were introduced; thus, the final rGO was low quality. This study also proposed a two-step reduction mechanism, where the first step is oxygen removal, which is a photochemical process, and the second step is the reorganization of the lattice from sp^3 to sp^2, which is thermally mediated [37].

The resolution of the pattern is critical for device miniaturization. One approach for significantly improving the resolution of LRG patterns involves the use of a two-beam system [38]. Here, the constructive and destructive interference of two laser beams on the surface is responsible for creating a pattern (Figure 3a), as the reduction takes place only in the periodic regions of the surface where the two beams add constructively, while no reduction happens where the two beams cancel each other. In this way, lines narrower than 1 μm can be produced (Figure 3b) [38].

While the studies presented so far are relative to GO films that were formed by drop-casting on a substrate, LS can also be achieved from a GO solution [39,40]. This was achieved again using a ns laser at 248 nm [39] or at 532 nm [40], which induces loss of oxygen as observed by XPS, but there is no graphenization as there is no significant change in the Raman spectrum. While this might appear to be in contrast with the results presented above [37], it must be noted that this is a solution process and no direct comparison should be made as the underlying reaction mechanisms could be different.

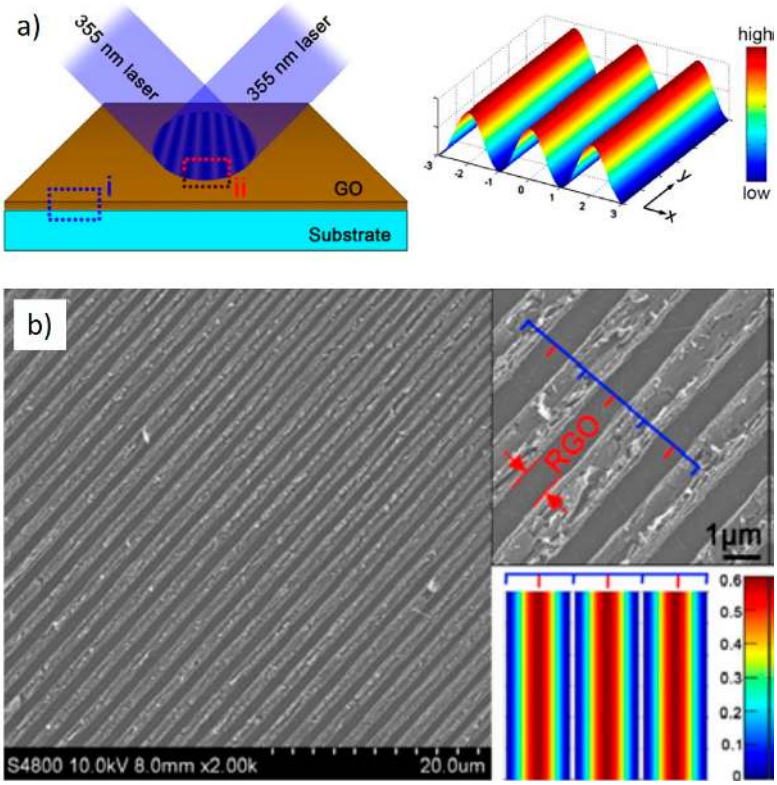

Figure 3. (**a**) Schematics and working principle of a dual beam laser system; (**b**) SEM images of rGO pattern obtained by the dual beam laser system. Reproduced with permission from Ref. [38]. Copyright 2012, Elsevier.

LIG can be obtained from a variety of sources. The first report appeared in 2014, as polyimide (PI) was used as source material [21]. Here, the authors used a CO_2 laser (10.6 μm wavelength) at 3.6 W power to make patterns onto PI. Such patterns showed loss of oxygen by XPS and the formation of graphene by Raman spectroscopy. The process was repeated on polyetherimide (PEI), although rGO quality was lower than on PI [21]. While the IR laser in the latter study could only produce patterns with a resolution limited to the order of several tens of micrometers, this can be reduced by using lasers in the visible spectrum, i.e., at shorter wavelengths [31]. Indeed, using a 405 nm laser, the resolution of the pattern could be reduced to 10–20 μm. PEI was also used to make nanocomposites with polycarbonate (PC). Here, a blend of the two polymers was exposed to a CO_2 laser and only PEI was converted to graphene, yielding a nanocomposite [41]. The same process was applied to sulfonated polymers to produce sulfur-doped porous graphene structures [42], which is of particular interest as such polymers are widely used in the technology industry. A sulfonated polymer, i.e., sulfonated poly(ether ketone) (SPEEK) was also used by Lamberti et al. to produce LIG using a CO_2 laser in order to obtain a flexible conductive material, which was then used as an electrode for supercapacitors [43]. Here, the conversion into graphene, not possible in conventional PEEK, is proposed to be mediated by sulfur, through reticulation by sulfonic group degradation and oxidative dehydrogenation by sulfur reaction [43]. A composite based on carboxymethyl cellulose (CMC) was developed by mixing PI powder in water solution and was deposited by vacuum filtration [44]. The mixture was then exposed to laser writing using a CO_2 laser at 10.6 μm.

Beside polymers, LIG can be obtained by LS using natural sources. This was reported for the first time by Ye et al. [22], who used a CO_2 laser on different types of wood under a controlled reducing atmosphere rich in H_2 (>50%). The formation of graphene is supported by XPS and Raman spectroscopy. The authors suggest that a high content of lignin in

the starting material is needed to achieve the best graphene formation [22]. If wood is impregnated by a solution containing a metal salt, the LS process, carried out in Ar atmosphere, not only induces the formation of graphene but also reduces the metal ions to form metal nanocrystals, ultimately making a graphene–metal nanocomposite [45], suitable for application in electrocatalysis, as will be discussed in the next section. It was then noted that other natural materials have higher lignin content than wood, and may thus be suitable for the formation of LIG. Indeed, Chyan et al. proposed to apply LS to food sources such as potato skins, coconut shells, or other natural materials such as cork [46]. Due to the higher lignin content, the LS process can be carried out in ambient atmosphere. The authors of this study have investigated an even wider range of both polymers and natural materials and have concluded that virtually any carbon source can be either converted to graphene or firstly transformed into amorphous carbon and then converted to graphene [46]. By multiple laser passes, they found that polymers with high melting temperature or that are cross-linked were directly converted into graphene, whilst vinyl polymers and other natural materials were first converted to amorphous carbon and then to graphene.

Moreover, the initial conversion to amorphous carbon could be obtained by any method, not just by laser irradiation [46]. The same multi-pass approach was later proposed by the same group to obtain LIG from an acrylate-based positive photoresist [47]. A two-step approach was also proposed by Li et al. [48] starting from silk fabric, as they first heated the material to 350 °C and then exposed the same to a laser scribing process to obtain LIG, as witnessed by Raman spectroscopy. Because lignin is a common industrial byproduct, Mahmood et al. demonstrated the direct conversion of such material to graphene using laser writing [49]. Molecular dynamics (MD) simulations have been carried out on the laser irradiation of PI, showing that at temperatures above 2400 K, pressures above 3 GPa are induced, allowing the formation of graphene clusters containing rings formed by five, six, or seven elements [50]. Such clusters, still according to MD simulations, have non-carbon atoms bonded at the edges, suggesting that these could allow the formation of intermediates that ultimately induce the formation of rings [50].

While we have discussed how a controlled atmosphere allows the formation of LIG which could not otherwise be formed, such an approach was also used to control or improve the properties of LRG and LIG. The first report of such an approach was published in 2010 by Zhou et al. [14], who used direct laser writing by a continuous laser at 663 nm in air to make patterns by oxidative burning of GO films, then irradiating in N_2 atmosphere to obtain LRG. Thus, in this case, while laser irradiation in air caused GO etching, in N_2 atmosphere it caused GO reduction [14]. Sokolov et al. irradiated GO films with 355 nm and 532 nm continuous laser in air and N_2, and noted by Raman spectroscopy that irradiation in N_2 atmosphere yielded rGO with less disorder [51]. Further studies were expanded to other atmospheres such as Ar and argon/H_2 (95:5) using a 405 nm continuous laser source [52]. Here, it was found by Raman spectroscopy that while Ar atmosphere produces better rGO than N_2, the results obtained in Ar/H_2 are the most promising due to the presence of 5% H_2 that makes the atmosphere slightly reducing and thus more suitable for GO reduction (Figure 4) [52]. The Ar-based environments were subject to further investigation relative to the LS conditions. It was found that the slower the laser writing speed (1.2 mm/s), the worse the conditions for reducing GO, while the fastest speed (5.9 mm/s) was optimal for Ar/H_2 atmosphere and an intermediate one (2.7 mm/s) was optimal for Ar. It was also found that a second laser pass yields a further improvement in GO reduction [53].

Li et al. investigated the formation of LIG from PI in different atmospheres [54]. While from Raman spectroscopy they also observed a better graphene quality in Ar or H_2 atmosphere, they also studied the surface properties of the obtained GO by contact angle measurements. It was found that while the produced samples generally show superhydrophilicity, with contact angle close to zero, when irradiating in a chamber with Ar or H_2 the material becomes superhydrophobic, with contact angle close to 150° (Figure 5) [54].

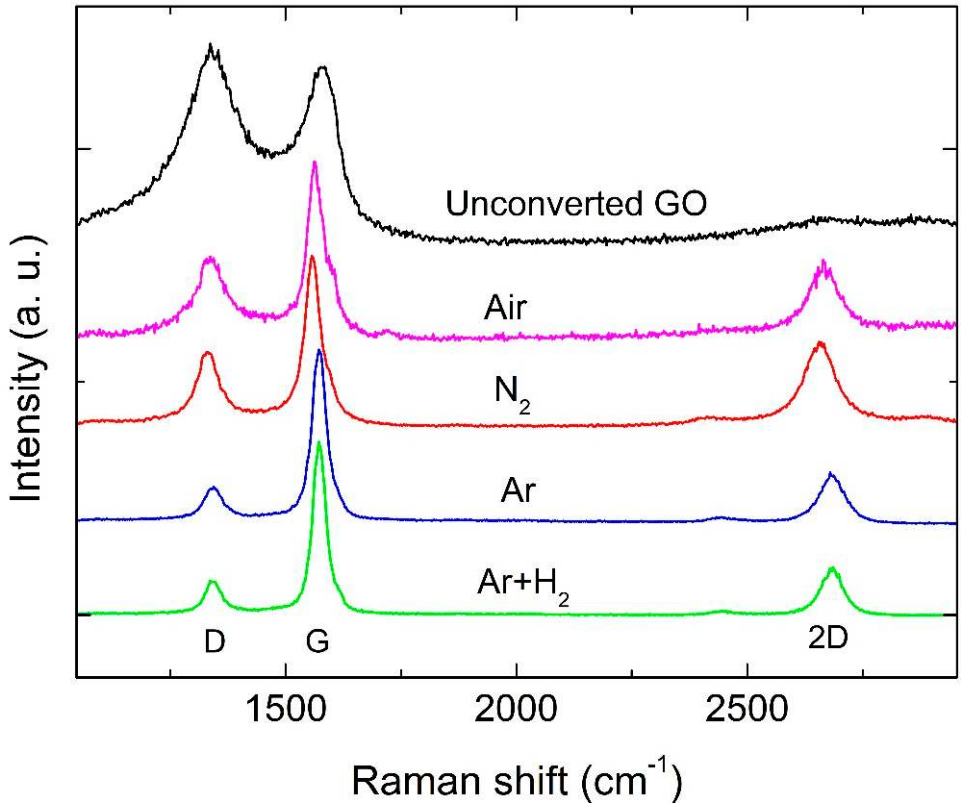

Figure 4. Raman spectra from LRG produced in different controlled atmospheres. Data adapted from Ref [52].

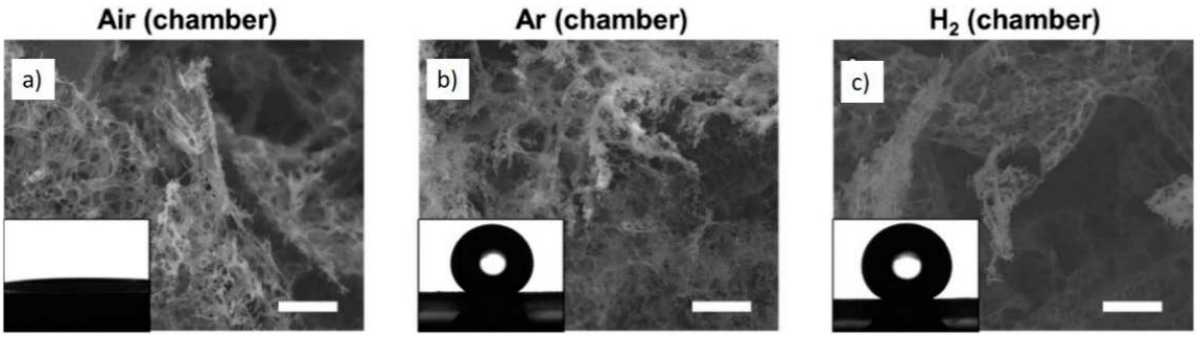

Figure 5. SEM images and contact angle measurements from LIG in (**a**) air; (**b**) Ar; and (**c**) H_2 controlled atmospheres. Reproduced with permission from Ref. [54]. Copyright 2017, Wiley.

3. Applications of Laser Synthesized Graphene

This section attempts to give a comprehensive overview of the applications reported for LSG, thus covering the most popular ones, such as, for example, sensing or supercapacitors, as well as some niche or futuristic applications, related to wearable technologies.

3.1. Humidity Sensing

Like most applications, relative humidity (RH) sensing exploits the conductive properties of rGO. This is mainly achieved by using rGO in two different ways. On the one hand, conductive rGO traces, surrounded by insulating GO, make the sensing element through the relative resistance variation ($\Delta R/R$) upon exposure to changing RH. On the other hand, the rGO conductive elements constitute the electrodes of a capacitor, in which the capacitive element is the non-reduced GO region between the electrodes. Hence, we can have resistive or capacitive sensing.

Resistive RH sensing was first reported in GO by Guo et al. [38] who produced an rGO pattern by the two-beam laser system described in the previous section and shown in Figure 3. They reported a ΔR of two orders of magnitude upon variation of RH from 11% to 95%. The system also showed a very fast response time (2 s) upon the same variation, but a slower recovery (100 s) upon the opposite path [38]. Capacitive RH sensing was reported by Cai et al. [55], who also were able to control the device operation through a smartphone, using a commercial oscilloscope application (Figure 6). The system showed a detection limit around 6% RH and very fast response (2 s) and recovery (4 s) time [55].

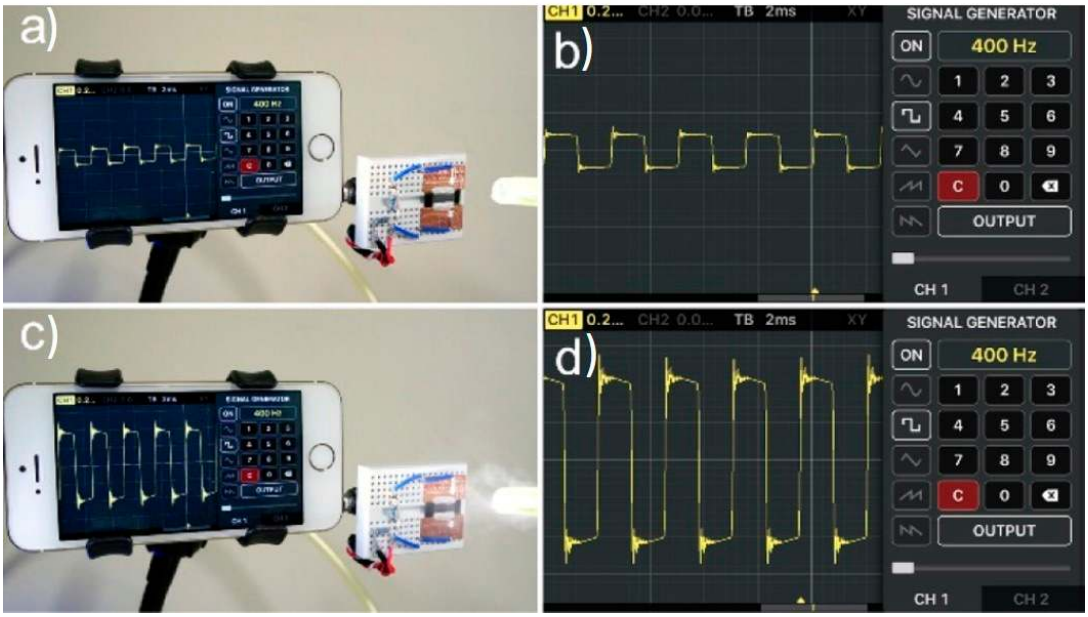

Figure 6. Photographic images of the smartphone/sensor setup (**a**,**c**) and the sensor response on the smartphone screen (**b**,**d**) upon turning a blowing mist on (**a**,**b**) and off (**c**,**d**) towards the sensor. Reproduced with permission from Ref. [55]. Copyright 2018, American Chemical Society.

RH response from rGO obtained under different controlled atmospheres (air, N_2, Ar, Ar/H_2) was also investigated [52]. It was found that the highest $\Delta R/R$ (~10%) was given by rGO obtained in argon, with the lowest hysteresis. The system showed a response and recovery as fast as that of a commercial RH sensor, but it was only responsive between 0% and ~15% RH [52].

GO/rGO response to RH humidity changes was applied by Han et al. to make actuators [56]. Such devices exploit the opposite deformation of GO and rGO under the effect of humidity changes (Figure 7a,b), with more complex actions achieved by patterning regions of GO and rGO on the same substrates (Figure 7c) [56]. A different type of actuator was made by combining an LRG with an ionic polymer membrane in a sandwich-type structure, in which a GO paper sheet was laser scribed only on one side, in contact with the polymer membrane, and left pristine on the other side, remaining hydrophobic and liquid-impermeable (Figure 8a,b) [57]. The actuation was achieved through an electrical potential applied to the two GO/LRG sheets used as electrodes. This system has the advantage of durability compared to more traditional systems employing noble metal sheets as electrodes, which are subjected to cracking and consequent leaking from the inner material [57].

The only report on an RH sensor based on LIG, to the author's knowledge, was given by Stanford et al. [31]. Here, graphene lines were made very thin by a UV laser on a PI substrate so that they were almost invisible to the human eye. Such lines were used as electrodes and the current between two electrodes, through a 7 μm gap, was measured to detect human breath, with a 250 ms response time (Figure 9) [31].

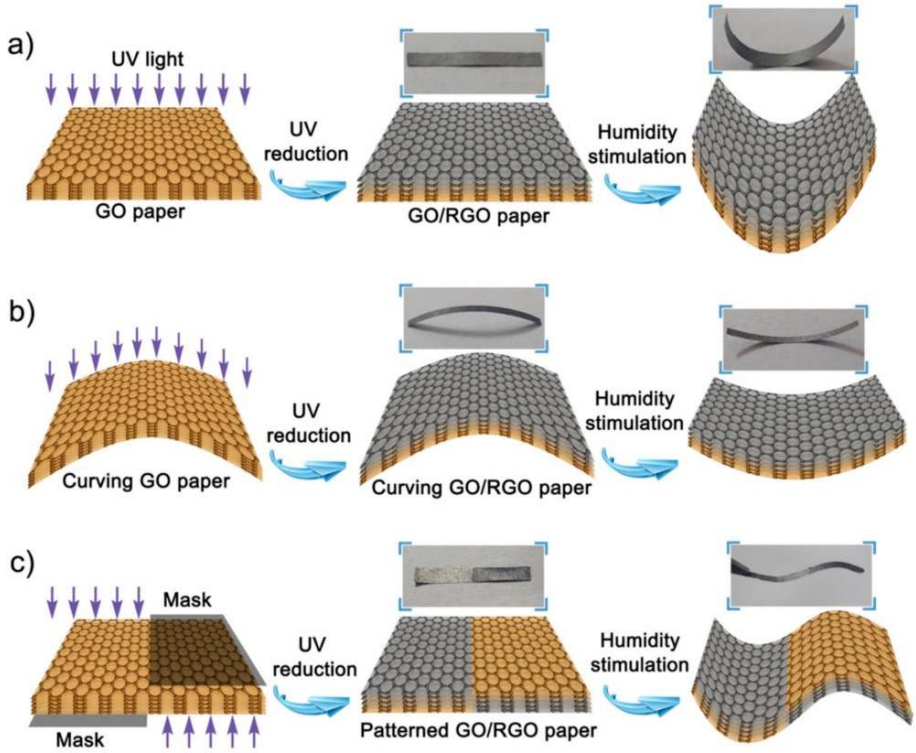

Figure 7. Working principle of a GO/rGO actuator based on (**a**) flat paper, (**b**) curving paper, (**c**) patterned GO/rGO paper. Reproduced with permission from Ref. [56]. Copyright 2015, Wiley.

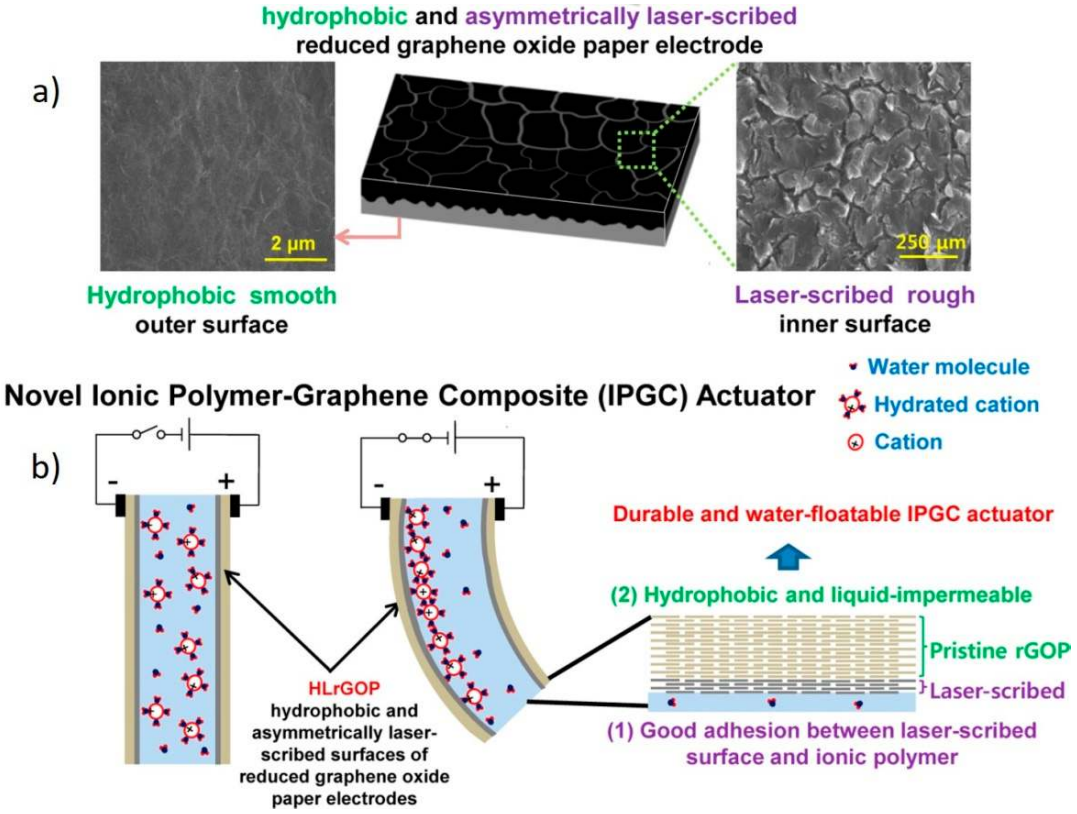

Figure 8. (**a**) GO sheet asymmetrically scribed to produce one hydrophobic interface and one hydrophilic interface. (**b**) Schematic representation of the structure and mechanism of LRG-based ionopolymer actuator. Reproduced with permission from Ref. [57]. Copyright 2014, American Chemical Society.

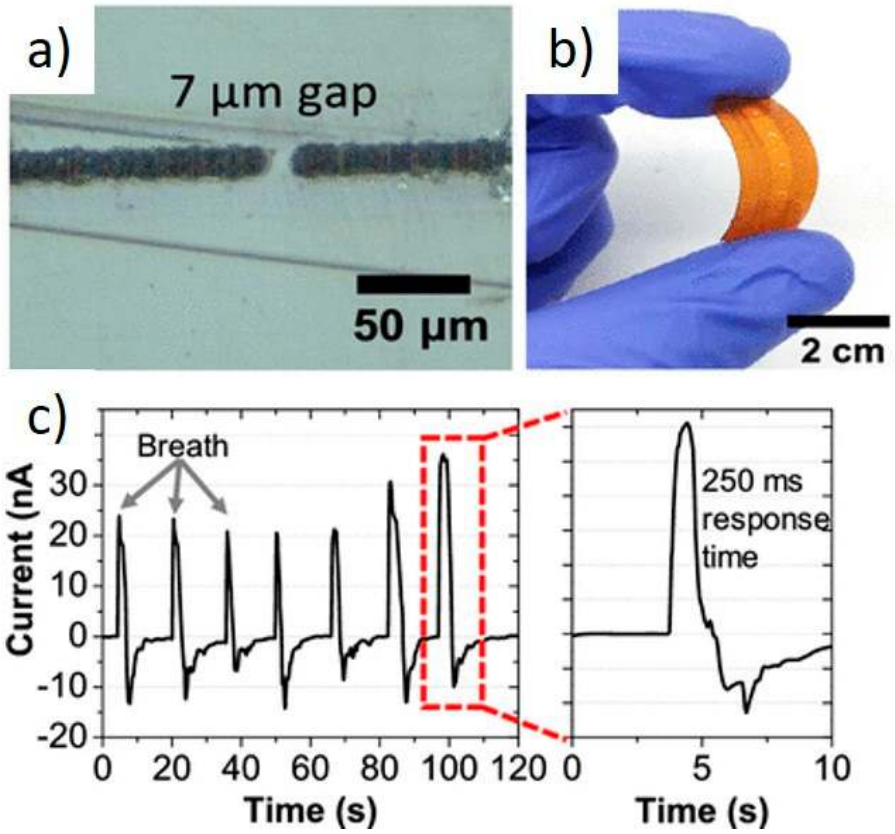

Figure 9. (**a**) Optical micrograph of the LIG electrode; (**b**) photographic image of the sensing device; (**c**) sensing response of the obtained device to human breath. Reproduced with permission from Ref. [31]. Copyright 2020, American Chemical Society.

3.2. Gas and Liquid Sensing

The general working principle of gas sensors based on LSG is the same as that outlined in Section 3.1 for RH sensors. In this case, to the author's knowledge, only resistive sensing was investigated. It is clear that the selectivity challenge associated with sensing systems based on nanomaterials equally applies to LSG systems. One gas sensing study using LRG was reported by Strong et al. for NO_2 sensing on flexible substrates [35]. However, the sensor response here was limited to $\Delta R/R < 1\%$ under exposure to 20 ppm NO_2. Multiple gas sensing was reported by Choi et al., who investigated H_2S, H_2, and ethanol as analytes [33]. The authors reported sensitivity in the region of 0.2% upon exposure to 20 ppm gas, and used principal component analysis to achieve selectivity from the gas response measurements [33].

LIG was used for flexible gas sensors by Stanford et al., who investigated a range of gases such as CO_2, O_2, N_2, H_2, argon, helium, with sensitivities reported up to 5% and detection limits estimated in the 100–1000 ppm range [31]. The authors of this study did not speculate on the selectivity of their system, although they showed the different response and recovery times for the gases, which through appropriate data analytics might provide species information in a field setting.

Liquid sensing has been proposed by Wang et al. [58], who characterized the $\Delta R/R$ response of LRG to a range of different liquids. It can be observed that the response is made of three stages, as shown in Figure 10: the first stage sees the $\Delta R/R$ increase due to the absorption of a drop of liquid within the porous structure of rGO; in the second stage $\Delta R/R$ maintains constant for a short time, then in the third stage the liquid evaporates and the $\Delta R/R$ goes back to zero. This is repeated over 50 cycles showing robustness and repeatability [58].

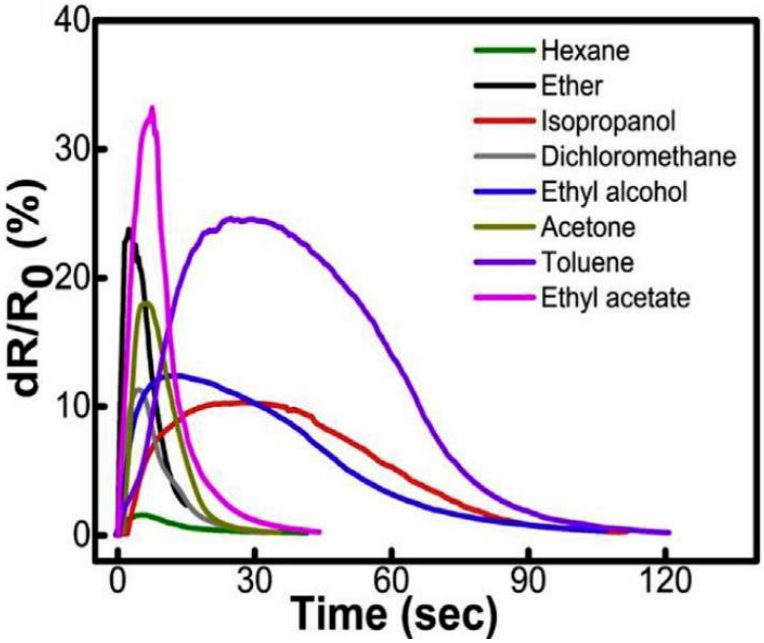

Figure 10. Electrical response of an LRG system under exposure to drops of different liquids. Reproduced with permission from Ref. [58]. Copyright 2019, Elsevier.

3.3. Strain Sensing

Strain sensors generally exploit a variation of the electrical properties of a material upon deformation of the material itself. These are generally evaluated by the gauge factor (GF), defined as $\frac{\Delta R/R_0}{\varepsilon}$, where ε is the applied strain ($\Delta L/L_0$). LRG has been demonstrated as a strain sensor by Tian et al. [59]. Here, rGO was obtained by DVD LightScribe process on a PET substrate. The authors showed the operation of a low GF system (0.11), with a linear relationship between R/R_0 and the strain, suitable for high deformations, where rGO was formed as a film, as well as high GF system (9.49) formed by an rGO microribbon, suitable for very small deformations [59]. The former shows repeatable operation at least up to 150 cycles, while the latter fails after 35 cycles.

A strain sensor based on an LIG stripe obtained from PI was demonstrated by Rahimi et al. [60]. Here, while the system showed robust repeatability at least up to 1000 cycles, the relationship between R/R_0 and the strain is logarithmic, and the GF is thus not constant. This is attributed to a very high resistance change at strains closer to 100%. While the authors admit that this might require more complex circuitry in a real-life system, they propose that the system is promising for human body applications where high strain sensing is critical, and demonstrate this by applying the sensor to a hand glove and measuring electrical properties during hand motion (Figure 11a) [60]. A similar application was demonstrated in Ref. [61] where graphene was obtained within a polydimethylsiloxane (PDMS) matrix and tested against different parts of the body, including facial muscles for facial expression and fingers and biceps for body movement. An LIG pattern on PI was transfer-printed onto a fiberglass composite, allowing in situ structural health monitoring of components, with no need for external bonding [62]. Here, the system shows a strain gauge between 0.5 and 1.3 and is able to detect both dynamic and quasi-static strain [62]. Carvalho et al. went a step further and demonstrated heart beat detection using LIG from PI (Figure 11c) [63]. Sun et al. went even further and developed a system, based on porous LIG made from PI, that is able to detect electrophysiological processes that produce signals commonly known as electroencephalogram (EEG), electrocardiogram (ECG), and electromyogram (EMG) (Figure 11b) [64].

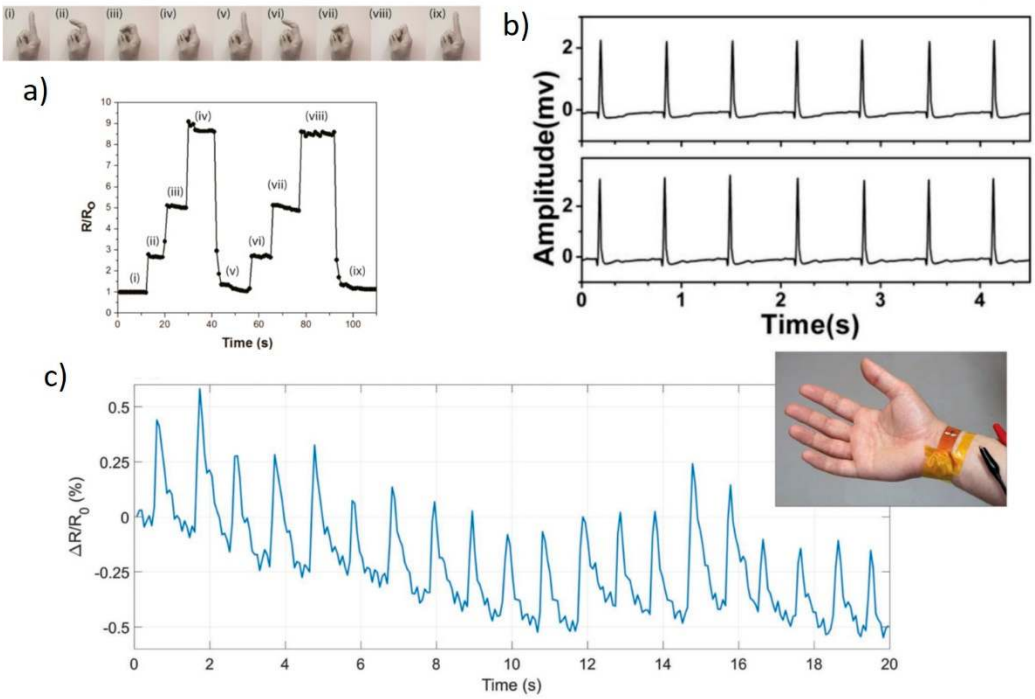

Figure 11. (**a**) LIG-based system to detect motion of a finger. Reproduced with permission from Ref. [60]. Copyright 2015, American Chemical Society. (**b**) ECG from an LIG-based system. Reproduced with permission from Ref. [64]. Copyright 2018, Wiley. (**c**) Heart beat detection from an LIG system. Reproduced with permission from ref. [63]. Copyright 2018, Wiley.

Overall, strain sensing has been extensively studied, especially for LIG, and a number of real-life applications have been demonstrated as proof of concept, mainly in the healthcare field. Thus, with appropriate scaling up of the production, such systems may potentially be ready to compete in the market with existing devices.

Somehow related to strain sensing is sound sensing, as an "artificial throat" was demonstrated by Tao et al. as a device that can both produce and detect sound [65]. Indeed, as the device, made from LIG, is exposed to AC voltage, the material produces sound waves generated by expansion of air, induced by the periodic joule heating. On the other hand, under a low bias voltage, the device can detect the vibrations of throat cords through a resistance change, if applied on a human tester throat [65]. In the latter case the device can distinguish different sounds such as humming, coughing, screaming, as well as movements such as swallowing and nodding, acting in this case as a strain sensing device.

3.4. Biosensing

Biosensing typically refers to the detection of molecules or biomolecules using a device employing a biological component. LIG has been identified as a suitable component for biosensing due to the porous structure allowing a high surface area, similar to other sensing applications. One of the first reports that appeared demonstrated the detection of Bisphenol-A [66], a molecule used in many industrial applications that is often found in the environment. The detection, down to femto- or attomolar concentrations, involved the functionalization of the LIG surface by aptamers, i.e., oligonucleotides or peptides that bind specifically to the target molecule. Here, the LIG was patterned as interdigitated electrodes to provide a capacitive sensing through an AC electroosmotic effect [66]. LIG decorated by Pt nanoparticles was used for the detection of ascorbic acid (AA), dopamine (DA), and uric acid (UA) [67]. This was achieved by electrochemical sensing using cyclic voltammetry and the limit of detection was of the order of the micromolar. Later, the same group used LIG to demonstrate the detection of thrombin [68], an enzyme that induces coagulation and may cause thrombosis. Here, LIG surface was functionalized by 1-pyrenebutyric acid that subsequently attached an aptamer for thrombin. The system uses a redox marker such

as hexacyanoferrate(III) ($[Fe(CN)_6]^{3-}$) that upon binding of thrombin to the aptamer is inhibited to reach the electrodes and causes a current drop [68], as schematized in Figure 12.

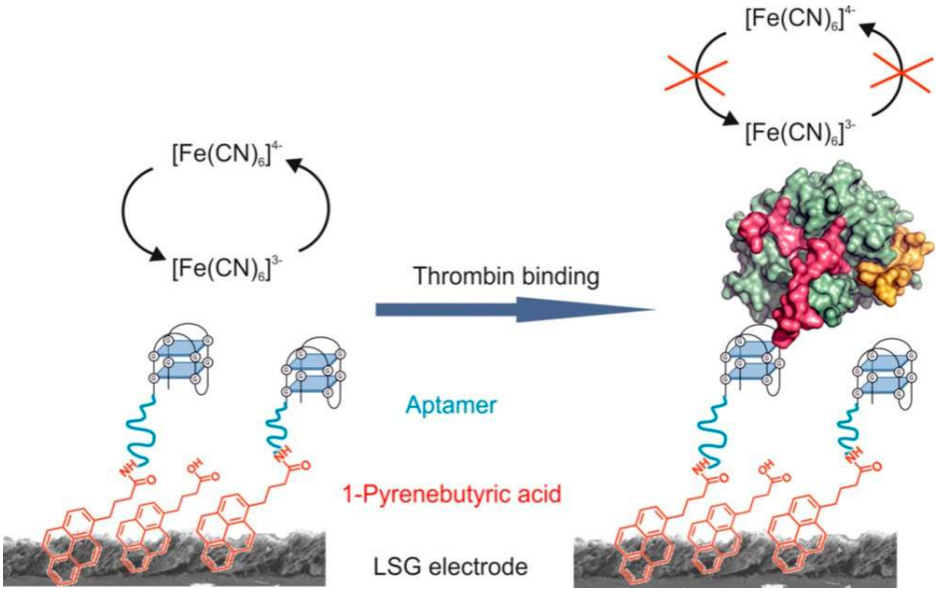

Figure 12. An example of aptamer-based biosensing on a laser-scribed graphene (LSG) or LIG electrode. Reproduced with permission from Ref. [68]. Copyright 2017, American Chemical Society.

A DA sensor has recently been demonstrated by Santos et al., where LIG is used without further functionalization [69]. LIG decorated with Cu nanocubes, deposited by electroplating, was used for the detection of biogenic amines [70], which are known as indicators of food degradation. Still related to food quality, Soares et al. proposed an LIG-based detection method for salmonella [71]. This is achieved through binding salmonella antibodies to the LIG surface and using electrochemical impedance spectroscopy for device characterization. Marques et al. proposed a dual LIG-based detector for AA and amoxicilline (AMOX) sensing, two ingredients found in fish farms that can leak into the outer environment [72]. Table 1 summarizes the findings from this section with the relevant sensor information.

Table 1. Summary of the key properties of biosensing systems based on laser-scribed graphene (LSG).

Author and Ref.	Analyte	Functionalization Type	Limit of Detection
Cheng [66]	Bisphenol-A	Aptamer	Atto-/Femtomolar
Fenzl [68]	Thrombin	Aptamer	Picomolar
Marques [72]	AA, AMOX	Polymers	Nanomolar
Nayak [67]	AA, DA, UA	Pt nanoparticles	Micromolar
Santos [69]	DA	-	Sub-micromolar
Soares [71]	Salmonella	Antibodies	13 colony-forming units
Vanegas [70]	Biogenic amines	Cu nanocubes	Micromolar

3.5. Pressure and Temperature Sensing

Pressure sensing has been demonstrated by Kazemzadeh et al. for LRG based on the piezoresistive response from the obtained rGO pattern, as a voltage output can be measured from the material as pressure is applied, once appropriate circuit elements are connected [73]. Indeed, applying pressure on the system induces more extended contact between graphene layers, thus decreasing resistivity and increasing output voltage. The sensitivity reported here is 19 mV/kPa [73]. This appears to be a very promising outcome, which, if associated with the strain sensing ability that is also demonstrated, could pave the way towards wearable technology based on LRG.

The same group proposed a temperature sensor based on the same material, deposited by drop-casting between two sets of electrodes [74]. The authors observed a drop in resistance upon increasing temperature, and fitted the obtained data using the equation $R(T) = T(T0)(1 + \alpha\Delta T)$, where α is the temperature coefficient. However, while the temperature coefficient reported (-0.0024) was in line with other values reported for graphene, this was investigated over a limited temperature range (20–40 °C) [74]; thus, further investigations for this type of sensing activity are required on a more extended temperature range.

3.6. Energy Storage

Energy storage has probably been the most sought after application for LSG since the first graphene-based supercapacitors were demonstrated. LSG-based supercapacitors are typically made of a couple of electrodes made of graphene and an insulator layer containing an electrolyte, thus working as a double-layer supercapacitor. The charge storage is thus non-Faradaic, as the accumulation is electrostatic and does not require any redox, just the formation of an electric double layer by the electrolyte. This can be achieved in two configurations. The first is an in-plane configuration, which is the most used, where LSG is patterned to form two interdigitated electrodes, while the region in between is filled with electrolyte (Figure 13a). A sandwich configuration is also sometimes used, in which layers of LSG alternate with electrolyte layers (Figure 13b).

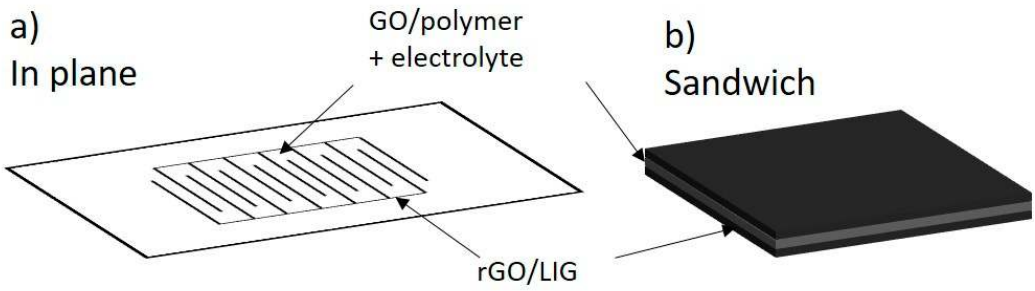

Figure 13. Schematization of the possible LSG-based supercapacitor configuration. (**a**) In-plane configuration where LSG form interdigitated electrodes; (**b**) sandwich configuration where LSG forms two plane electrodes with an electrolyte layer in between.

Such systems are typically characterized by cyclic voltammetry and charge-discharge galvanostatic measurements. Cyclability is usually also investigated by repeating such measurements, especially charge-discharge experiments, a multiple number of times. The key parameters are areal capacitance (usually $mFcm^{-2}$), power density ($mWcm^{-2}$ or Wcm^{-3}), and discharge time. Also important is the number of charge/discharge cycles investigated, which is an indication of the longer term stability of the device. The configurations and properties of supercapacitors made from LSG are summarized in Table 2. Here we observe that most devices are developed in the in-plane configuration and use an H_2SO_4/PVA electrolyte. For LRG, specific capacitances are reported in a 2–5 $mFcm^{-2}$ range, although a significant increase is given by graphene functionalization, for example with polyaniline [75]. The range is broader for LIG, where the highest are 361 and 320 $mFcm^{-2}$. However, functionalization again provides a significant boost to capacitance, with an impressive 2412 $mFcm^{-2}$ for polypyrrole functionalization [76]. Most reported devices show high charge/discharge cycle stability within thousands of cycles. While most power densities are reported in a 2–12 $mWcm^{-2}$ or 2–4 Wcm^{-3}, El-Kady et al. report a power density of 200 Wcm^{-3} [36], higher than any other supercapacitor. They also identify a trend in which the supercapacitor performance improves with electrode dimensions being reduced to the microscale.

Table 2. Key information from reports on LSG application for energy storage. PVA: polyvinyl alcohol. TEABF4: tetraethylammonium tetrafluoroborate. PANI: polyaniline. PPy: polypyrrole.

Author and Ref.	Configuration/Material	Electrolyte	Specific Capacitance	Power Density (Max)	Discharge Time (Max)	Stability (Cycles)
Cai [77]	In-plane/GO	H_2SO_4/PVA	3 $mFcm^{-2}$	-	60 s (0.05 $mAcm^{-2}$)	1000
El-Kady [19]	Sandwich/GO	H_3PO_4/PVA	5 $mFcm^{-2}$	3 Wcm^{-3}	10 s	10,000
El-Kady [36]	In-plane/GO	H_2SO_4/PVA	2.35 $mFcm^{-2}$	200 Wcm^{-3}	30 s	10,000
Gao [78]	In-plane + Sandwich/GO	Na_2SO_4 or $TEABF_4$	3 $mFcm^{-2}$	2.4 Wcm^{-3}	-	10,000
Laelabadi [75]	In-plane/GO + PANI	H_2SO_4/PVA	72 $mFcm^{-2}$	81.4 $mWcm^{-3}$	3000 s (35 μAcm^{-2})	1000
Lamberti [43]	In-plane/LIG	Na_2SO_4	0.34 $mFcm^{-2}$	0.01 $mWcm^{-2}$	200 s (0.625 μAcm^{-2})	-
Li [20]	In-plane/LIG	LiCl/PVA or H_2SO_4/PVA	361 $mFcm^{-2}$	11.8 $mWcm^{-2}$/2.89 Wcm^{-3}	150 s (0.25 $mAcm^{-2}$)	2000
Li [54]	In-plane/LIG	H_2SO_4/PVA	37 $mFcm^{-2}$	2 $mWcm^{-2}$	15 s (0.5 $mAcm^{-2}$)	-
Lin [21]	In-plane/LIG	H_2SO_4/ionic liquid	4 $mFcm^{-2}$	9 $mWcm^{-2}$/3 Wcm^{-3}	25 s (0.2 $mAcm^{-2}$)	9000
Liu [79]	In-plane/LIG + Fe_3O_4	H_2SO_4/PVA	719 $mFcm^{-2}$	0.3 $mWcm^{-2}$	-	900
Mahmood [49]	In-plane/LIG	H_2SO_4/PVA	0.88 $mFcm^{-2}$	25μWcm^{-2}	60 s (0.01 $mAcm^{-2}$)	10,000
Peng [80]	Sandwich/LIG	H_2SO_4/PVA	9 $mFcm^{-2}$	9 $mWcm^{-2}$/4 Wcm^{-3}	30 s (0.5 $mAcm^{-2}$)	8000
Peng [81]	In-plane/LIG	H_2SO_4/PVA	16.5 $mFcm^{-2}$	4 Wcm^{-3}	9 s (1 $mAcm^{-2}$)	12,000
Song [82]	In-plane/LIG	potassium polyacrylate/KOH gel electrolyte	0.79 $mFcm^{-2}$	-	7 s (75 μAcm^{-2})	10,000
Ye [22]	In-plane/LIG	KOH	320 $mFcm^{-2}$	-	600 s (1 $mAcm^{-2}$)	400
Yu [76]	In-plane/LIG + PPy	H_2SO_4/PVA	2412 $mFcm^{-2}$	0.325 $mWcm^{-2}$	4000 s (0.5 $mAcm^{-2}$)	10,000
Yuan [44]	In-plane/LIG	H_2SO_4/PVA	60.6 $mFcm^{-2}$	-	200 s (0.5 $mAcm^{-2}$)	20,000

3.7. Electrocatalysis

One interesting application for LSG that has been proposed is where this is employed as catalyst for electrochemical reactions, i.e., used as an electrocatalyst. In particular, oxygen evolution reactions (OER) are of special interest because of the technological implications regarding water splitting or fuel cells [83,84], to name a few. Typically, the most efficient materials are noble metals and metal oxides [85]. It has already been mentioned that cedar wood impregnated by metal salts solution is an effective source for LIG-metal nanocomposites, as the laser not only converts cedar wood into graphene but also reduces metal ions into nanocrystals. Such material shows electrocatalytic activity towards OER [45]. The interest in this process is in using, instead of noble metals, more common ones such as Ni and Fe, as well as an overpotential just below 300 mV (at 10 $mAcm^{-2}$ current density) [45]. A significant step further was achieved by Zhang et al., who proposed a metal-free electrocatalyst using an oxidized LIG, in which the oxidization, with further introduction of oxygen-containing functional groups, was achieved by oxygen plasma treatment [86]. Such functional groups, introduced by the plasma treatment, provide active sites as well as facilitate the adsorption of reaction intermediates, thus lowering the activation energy for the OER. The authors report that LIG itself is already active for OER, but introducing the oxygen-containing groups produces a significantly lower onset potential of 260 mV [86]. H_2O_2 has also generated technological interest as part of rocket propellants and fuel cells, besides a more traditional use as a strong oxidant and disinfectant. Singh et al. propose the use of sulfonated LIG for the electrocatalytic production of H_2O_2 in Na_2SO_4 and NaCl as electrolytes [42].

3.8. Environmental Applications

The ability of graphene to destroy or prevent the proliferation of bacteria and other microorganisms has been proven since the beginning of the last decade [87]. Such function has also been demonstrated for LIG. Singh et al. have shown that LIG can serve the double role of anti-fouling surface as well as an antibacterial surface when acting as an electrode [88]. Tested against *Pseudomonas aeruginosa* under biofilm growth conditions, no biofilm growth was detected on LIG. The antimicrobial activity was demonstrated on both LIG surface and a powder obtained by scraping LIG off the original surface. The performance increased as a voltage up to 2.5 V was applied to LIG on the surface, acting as electrode, compared with the powder [88]. Such function was enhanced using the S-doped LIG [42].

A similar ability was demonstrated by Stanford et al., who showed that LIG can be utilized as a self-sterilizing bacterial air filter [89]. Indeed, as airflow passes through an LIG porous structure, it is able to retain microorganisms (Figure 14a). By applying a voltage to the material, joule heating can reach around 300 °C, which can kill any microorganisms present on the filter, thus achieving sterilization (Figure 14b) [89].

The adsorption of organic dye compounds by LIG powders was demonstrated by Rathinam et al. [90]. Here, methylene blue and methyl orange were used as sample molecules for cationic and anionic organic water pollutants, respectively. The adsorption mechanism was attributed to π-π interactions and electrostatic interactions. By varying pH, the adsorption capacity for methylene blue held very high, between 88% and 100% between pH = 2 and pH = 10, while for methyl orange the adsorption capacity decreased by increasing pH, but was still >70% at pH = 10 [90]. This system showed superior capacity in comparison to graphene oxide, which suffered at high pH. Furthermore, such system did not suffer interference from anions usually present in water such as chloride, sulfate, nitrate, and bicarbonate [90].

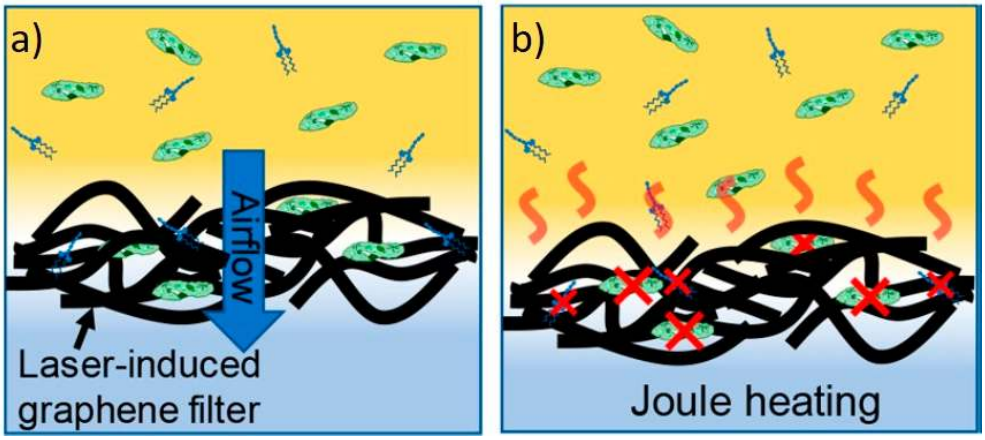

Figure 14. (**a**) Schematics of air filtration by LIG-based air filter. (**b**) Schematics of filter sterilization by joule heating. Reproduced with permission from Ref. [89]. Copyright 2019, American Chemical Society.

4. Conclusions and Perspectives

This review covers the broad range of synthetic conditions and the applications of graphene obtained by laser reduction of graphene oxide as well as induced by laser on other materials such as commercial polymers or natural sources. In particular, examples have been given on how different synthetic and processing conditions can influence the final properties of LSG, such as the reaction atmosphere, laser wavelength, light source, starting material composition. A wide range of applications has also been covered, including different types of sensing, energy storage, electrocatalysis, and environmental.

All applications presented are indeed very promising from a proof-of-concept standpoint. However, becoming a competing technology in the real market needs to take into account other factors such as cost, scalability, and competitiveness against other established technologies. Hence, applications that should compete with technologies that already offer cheap alternatives, such as RH, temperature or pressure sensing, as well as some gas sensing, are bound to remain at a proof-of-concept stage. On the other hand, applications that have generally been developed more recently and are thus farther from maturity, for example, those related to wearable technologies or biosensing, offer more space for new materials. Here is where LRG or LSG could find a path forward to move from the lab to the market. This is the case for the strain sensing and biosensing applications or the energy storage solutions that have been outlined in Section 3, where nanomaterials, and graphene in particular, offer a clear value add that can speed up both technical performance and scaling up efforts.

Funding: This research received no external funding.

Data Availability Statement: Not applicable.

Conflicts of Interest: The author declares no conflict of interest.

References

1. Novoselov, K.S.; Jiang, D.; Schedin, F.; Booth, T.J.; Khotkevich, V.V.; Morozov, S.V.; Geim, A.K. Two-dimensional atomic crystals. *Proc. Natl. Acad. Sci. USA* **2005**, *102*, 10451–10453. [CrossRef]
2. Novoselov, K.S.; Geim, A.K.; Morozov, S.V.; Jiang, D.; Katsnelson, M.I.; Grigorieva, I.V.; Dubonos, S.V.; Firsov, A.A. Two-dimensional gas of massless Dirac fermions in graphene. *Nature* **2005**, *438*, 197–200. [CrossRef]
3. Novoselov, K.S.; Geim, A.K.; Morozov, S.V.; Jiang, D.; Zhang, Y.; Dubonos, S.V.; Grigorieva, I.V.; Firsov, A.A. Electric Field Effect in Atomically Thin Carbon Films. *Science* **2004**, *306*, 666–669. [CrossRef]
4. Reina, A.; Jia, X.; Ho, J.; Nezich, D.; Son, H.; Bulovic, V.; Dresselhaus, M.S.; Kong, J. Large Area, Few-Layer Graphene Films on Arbitrary Substrates by Chemical Vapor Deposition. *Nano Lett.* **2009**, *9*, 30–35. [CrossRef]
5. Li, X.; Cai, W.; An, J.; Kim, S.; Nah, J.; Yang, D.; Piner, R.; Velamakanni, A.; Jung, I.; Tutuc, E.; et al. Large-Area Synthesis of High-Quality and Uniform Graphene Films on Copper Foils. *Science* **2009**, *324*, 1312. [CrossRef]

6. Kim, K.S.; Zhao, Y.; Jang, H.; Lee, S.Y.; Kim, J.M.; Kim, K.S.; Ahn, J.-H.; Kim, P.; Choi, J.-Y.; Hong, B.H. Large-scale pattern growth of graphene films for stretchable transparent electrodes. *Nature* **2009**, *457*, 706–710. [CrossRef]
7. Bae, S.; Kim, H.; Lee, Y.; Xu, X.; Park, J.-S.; Zheng, Y.; Balakrishnan, J.; Lei, T.; Ri Kim, H.; Song, Y.I.; et al. Roll-to-roll production of 30-inch graphene films for transparent electrodes. *Nat. Nanotechnol.* **2010**, *5*, 574–578. [CrossRef]
8. Hernandez, Y.; Nicolosi, V.; Lotya, M.; Blighe, F.M.; Sun, Z.; De, S.; McGovern, I.T.; Holland, B.; Byrne, M.; Gun'Ko, Y.K.; et al. High-yield production of graphene by liquid-phase exfoliation of graphite. *Nat. Nanotechnol.* **2008**, *3*, 563–568. [CrossRef]
9. Lotya, M.; Hernandez, Y.; King, P.J.; Smith, R.J.; Nicolosi, V.; Karlsson, L.S.; Blighe, F.M.; De, S.; Wang, Z.; McGovern, I.T.; et al. Liquid Phase Production of Graphene by Exfoliation of Graphite in Surfactant/Water Solutions. *J. Am. Chem. Soc.* **2009**, *131*, 3611–3620. [CrossRef]
10. Lotya, M.; King, P.J.; Khan, U.; De, S.; Coleman, J.N. High-Concentration, Surfactant-Stabilized Graphene Dispersions. *ACS Nano* **2010**, *4*, 3155–3162. [CrossRef]
11. Bourlinos, A.B.; Georgakilas, V.; Zboril, R.; Steriotis, T.A.; Stubos, A.K.; Trapalis, C. Aqueous-phase exfoliation of graphite in the presence of polyvinylpyrrolidone for the production of water-soluble graphenes. *Solid State Commun.* **2009**, *149*, 2172–2176. [CrossRef]
12. Hummers, W.S.; Offeman, R.E. Preparation of Graphitic Oxide. *J. Am. Chem. Soc.* **1958**, *80*, 1339. [CrossRef]
13. Dreyer, D.R.; Park, S.; Bielawski, C.W.; Ruoff, R.S. The chemistry of graphene oxide. *Chem. Soc. Rev.* **2010**, *39*, 228–240. [CrossRef]
14. Zhou, Y.; Bao, Q.; Varghese, B.; Tang, L.A.L.; Tan, C.K.; Sow, C.-H.; Loh, K.P. Microstructuring of Graphene Oxide Nanosheets Using Direct Laser Writing. *Adv. Mater.* **2010**, *22*, 67–71. [CrossRef]
15. Ray, S.C. (Ed.) Chapter 2—Application and Uses of Graphene Oxide and Reduced Graphene Oxide. In *Applications of Graphene and Graphene-Oxide Based Nanomaterials*; William Andrew Publishing: Oxford, UK, 2015; pp. 39–55. [CrossRef]
16. Stankovich, S.; Dikin, D.A.; Piner, R.D.; Kohlhaas, K.A.; Kleinhammes, A.; Jia, Y.; Wu, Y.; Nguyen, S.T.; Ruoff, R.S. Synthesis of graphene-based nanosheets via chemical reduction of exfoliated graphite oxide. *Carbon* **2007**, *45*, 1558–1565. [CrossRef]
17. Stankovich, S.; Piner, R.D.; Chen, X.; Wu, N.; Nguyen, S.T.; Ruoff, R.S. Stable aqueous dispersions of graphitic nanoplatelets via the reduction of exfoliated graphite oxide in the presence of poly(sodium 4-styrenesulfonate). *J. Mater. Chem.* **2006**, *16*, 155–158. [CrossRef]
18. Zhang, Y.; Guo, L.; Wei, S.; He, Y.; Xia, H.; Chen, Q.; Sun, H.-B.; Xiao, F.-S. Direct imprinting of microcircuits on graphene oxides film by femtosecond laser reduction. *Nano Today* **2010**, *5*, 15–20. [CrossRef]
19. El-Kady, M.F.; Strong, V.; Dubin, S.; Kaner, R.B. Laser Scribing of High-Performance and Flexible Graphene-Based Electrochemical Capacitors. *Science* **2012**, *335*, 1326–1330. [CrossRef] [PubMed]
20. Li, L.; Zhang, J.B.; Peng, Z.W.; Li, Y.L.; Gao, C.T.; Ji, Y.S.; Ye, R.Q.; Kim, N.D.; Zhong, Q.F.; Yang, Y.; et al. High-Performance Pseudocapacitive Microsupercapacitors from Laser-Induced Graphene. *Adv. Mater.* **2016**, *28*, 838–845. [CrossRef]
21. Lin, J.; Peng, Z.W.; Liu, Y.Y.; Ruiz-Zepeda, F.; Ye, R.Q.; Samuel, E.L.G.; Yacaman, M.J.; Yakobson, B.I.; Tour, J.M. Laser-induced porous graphene films from commercial polymers. *Nat. Commun.* **2014**, *5*, 5714. [CrossRef]
22. Ye, R.; Chyan, Y.; Zhang, J.; Li, Y.; Han, X.; Kittrell, C.; Tour, J.M. Laser-Induced Graphene Formation on Wood. *Adv. Mater.* **2017**, *29*, 1702211. [CrossRef]
23. Algozeeb, W.A.; Savas, P.E.; Luong, D.X.; Chen, W.; Kittrell, C.; Bhat, M.; Shahsavari, R.; Tour, J.M. Flash Graphene from Plastic Waste. *ACS Nano* **2020**, *14*, 15595–15604. [CrossRef]
24. Kaidarova, A.; Kosel, J. Physical Sensors Based on Laser-Induced Graphene: A Review. *IEEE Sens. J.* **2021**, *21*, 12426–12443. [CrossRef]
25. Li, G. Direct laser writing of graphene electrodes. *J. Appl. Phys.* **2020**, *127*, 010901. [CrossRef]
26. Xu, Y.; Fei, Q.; Page, M.; Zhao, G.; Ling, Y.; Chen, D.; Yan, Z. Laser-induced graphene for bioelectronics and soft actuators. *Nano Res.* **2021**. [CrossRef] [PubMed]
27. Cheng, L.; Guo, W.; Cao, X.; Dou, Y.; Huang, L.; Song, Y.; Su, J.; Zeng, Z.; Ye, R. Laser-induced graphene for environmental applications: Progress and opportunities. *Mater. Chem. Front.* **2021**. [CrossRef]
28. Huang, L.; Su, J.; Song, Y.; Ye, R. Laser-Induced Graphene: En Route to Smart Sensing. *Nano-Micro Lett.* **2020**, *12*, 157. [CrossRef]
29. Ye, R.; James, D.K.; Tour, J.M. Laser-Induced Graphene: From Discovery to Translation. *Adv. Mater.* **2019**, *31*, 1803621. [CrossRef]
30. Wan, Z.; Streed, E.W.; Lobino, M.; Wang, S.; Sang, R.T.; Cole, I.S.; Thiel, D.V.; Li, Q. Laser-Reduced Graphene: Synthesis, Properties, and Applications. *Adv. Mater. Technol.* **2018**, *3*, 1700315. [CrossRef]
31. Stanford, M.G.; Zhang, C.; Fowlkes, J.D.; Hoffman, A.; Ivanov, I.N.; Rack, P.D.; Tour, J.M. High-Resolution Laser-Induced Graphene. Flexible Electronics beyond the Visible Limit. *ACS Appl. Mater. Interfaces* **2020**, *12*, 10902–10907. [CrossRef]
32. Cote, L.J.; Cruz-Silva, R.; Huang, J. Flash Reduction and Patterning of Graphite Oxide and Its Polymer Composite. *J. Am. Chem. Soc.* **2009**, *131*, 11027–11032. [CrossRef]
33. Choi, S.-J.; Kim, S.-J.; Kim, I.-D. Ultrafast optical reduction of graphene oxide sheets on colorless polyimide film for wearable chemical sensors. *NPG Asia Mater.* **2016**, *8*, e315. [CrossRef]
34. Trusovas, R.; Ratautas, K.; Račiukaitis, G.; Barkauskas, J.; Stankevičienė, I.; Niaura, G.; Mažeikienė, R. Reduction of graphite oxide to graphene with laser irradiation. *Carbon* **2013**, *52*, 574–582. [CrossRef]
35. Strong, V.; Dubin, S.; El-Kady, M.F.; Lech, A.; Wang, Y.; Weiller, B.H.; Kaner, R.B. Patterning and Electronic Tuning of Laser Scribed Graphene for Flexible All-Carbon Devices. *ACS Nano* **2012**, *6*, 1395–1403. [CrossRef] [PubMed]

36. El-Kady, M.F.; Kaner, R.B. Scalable fabrication of high-power graphene micro-supercapacitors for flexible and on-chip energy storage. *Nat. Commun.* **2013**, *4*, 1475. [CrossRef] [PubMed]
37. Arul, R.; Oosterbeek, R.N.; Robertson, J.; Xu, G.; Jin, J.; Simpson, M.C. The mechanism of direct laser writing of graphene features into graphene oxide films involves photoreduction and thermally assisted structural rearrangement. *Carbon* **2016**, *99*, 423–431. [CrossRef]
38. Guo, L.; Jiang, H.-B.; Shao, R.-Q.; Zhang, Y.-L.; Xie, S.-Y.; Wang, J.-N.; Li, X.-B.; Jiang, F.; Chen, Q.-D.; Zhang, T.; et al. Two-beam-laser interference mediated reduction, patterning and nanostructuring of graphene oxide for the production of a flexible humidity sensing device. *Carbon* **2012**, *50*, 1667–1673. [CrossRef]
39. Huang, L.; Liu, Y.; Ji, L.-C.; Xie, Y.-Q.; Wang, T.; Shi, W.-Z. Pulsed laser assisted reduction of graphene oxide. *Carbon* **2011**, *49*, 2431–2436. [CrossRef]
40. Buccheri, M.A.; D'Angelo, D.; Scalese, S.; Spanò, S.F.; Filice, S.; Fazio, E.; Compagnini, G.; Zimbone, M.; Brundo, M.V.; Pecoraro, R.; et al. Modification of graphene oxide by laser irradiation: A new route to enhance antibacterial activity. *Nanotechnology* **2016**, *27*, 245704. [CrossRef] [PubMed]
41. Yazdi, A.Z.; Navas, I.O.; Abouelmagd, A.; Sundararaj, U. Direct Creation of Highly Conductive Laser-Induced Graphene Nanocomposites from Polymer Blends. *Macromol. Rapid Commun.* **2017**, *38*, 1700176. [CrossRef]
42. Singh, S.P.; Li, Y.; Zhang, J.; Tour, J.M.; Arnusch, C.J. Sulfur-Doped Laser-Induced Porous Graphene Derived from Polysulfone-Class Polymers and Membranes. *ACS Nano* **2018**, *12*, 289–297. [CrossRef]
43. Lamberti, A.; Serrapede, M.; Ferraro, G.; Fontana, M.; Perrucci, F.; Bianco, S.; Chiolerio, A.; Bocchini, S. All-SPEEK flexible supercapacitor exploiting laser-induced graphenization. *2d Mater.* **2017**, *4*, 035012. [CrossRef]
44. Yuan, M.; Luo, F.; Wang, Z.; Li, H.; Rao, Y.; Yu, J.; Wang, Y.; Xie, D.; Chen, X.; Wong, C.-P. Facile and Scalable Fabrication of High-Performance Microsupercapacitors Based on Laser-Scribed In Situ Heteroatom-Doped Porous Graphene. *ACS Appl. Mater. Interfaces* **2021**, *13*, 22426–22437. [CrossRef] [PubMed]
45. Han, X.; Ye, R.; Chyan, Y.; Wang, T.; Zhang, C.; Shi, L.; Zhang, T.; Zhao, Y.; Tour, J.M. Laser-Induced Graphene from Wood Impregnated with Metal Salts and Use in Electrocatalysis. *ACS Appl. Nano Mater.* **2018**, *1*, 5053–5061. [CrossRef]
46. Chyan, Y.; Ye, R.; Li, Y.; Singh, S.P.; Arnusch, C.J.; Tour, J.M. Laser-Induced Graphene by Multiple Lasing: Toward Electronics on Cloth, Paper, and Food. *ACS Nano* **2018**, *12*, 2176–2183. [CrossRef]
47. Beckham, J.L.; Li, J.T.; Stanford, M.G.; Chen, W.; McHugh, E.A.; Advincula, P.A.; Wyss, K.M.; Chyan, Y.; Boldman, W.L.; Rack, P.D.; et al. High-Resolution Laser-Induced Graphene from Photoresist. *ACS Nano* **2021**. [CrossRef]
48. Li, Z.; Lu, L.; Xie, Y.; Wang, W.; Lin, Z.; Tang, B.; Lin, N. Preparation of Laser-Induced Graphene Fabric from Silk and Its Application Examples for Flexible Sensor. *Adv. Eng. Mater.* **2021**, 2100195. [CrossRef]
49. Mahmood, F.; Zhang, H.; Lin, J.; Wan, C. Laser-Induced Graphene Derived from Kraft Lignin for Flexible Supercapacitors. *ACS Omega* **2020**, *5*, 14611–14618. [CrossRef]
50. Dong, Y.; Rismiller, S.C.; Lin, J. Molecular dynamic simulation of layered graphene clusters formation from polyimides under extreme conditions. *Carbon* **2016**, *104*, 47–55. [CrossRef]
51. Sokolov, D.A.; Shepperd, K.R.; Orlando, T.M. Formation of Graphene Features from Direct Laser-Induced Reduction of Graphite Oxide. *J. Phys. Chem. Lett.* **2010**, *1*, 2633–2636. [CrossRef]
52. Scardaci, V.; Fichera, L.; Fragalà, M.E.; Tuccitto, N.; Marletta, G.; Compagnini, G. Reduction of Graphene Oxide by Laser Scribing in Different Atmospheres and Application in Humidity Sensing. *J. Nanomater.* **2020**, *2020*, 4946954. [CrossRef]
53. Scardaci, V.; Compagnini, G. Raman Spectroscopy Investigation of Graphene Oxide Reduction by Laser Scribing. *C* **2021**, *7*, 48. [CrossRef]
54. Li, Y.L.; Luong, D.X.; Zhang, J.B.; Tarkunde, Y.R.; Kittrell, C.; Sargunaraj, F.; Ji, Y.S.; Arnusch, C.J.; Tour, J.M. Laser-Induced Graphene in Controlled Atmospheres: From Superhydrophilic to Superhydrophobic Surfaces. *Adv. Mater.* **2017**, *29*, 1700496. [CrossRef] [PubMed]
55. Cai, J.; Lv, C.; Aoyagi, E.; Ogawa, S.; Watanabe, A. Laser Direct Writing of a High-Performance All-Graphene Humidity Sensor Working in a Novel Sensing Mode for Portable Electronics. *ACS Appl. Mater. Interfaces* **2018**, *10*, 23987–23996. [CrossRef]
56. Han, D.-D.; Zhang, Y.-L.; Liu, Y.; Liu, Y.-Q.; Jiang, H.-B.; Han, B.; Fu, X.-Y.; Ding, H.; Xu, H.-L.; Sun, H.-B. Bioinspired Graphene Actuators Prepared by Unilateral UV Irradiation of Graphene Oxide Papers. *Adv. Funct. Mater.* **2015**, *25*, 4548–4557. [CrossRef]
57. Kim, J.; Jeon, J.-H.; Kim, H.-J.; Lim, H.; Oh, I.-K. Durable and Water-Floatable Ionic Polymer Actuator with Hydrophobic and Asymmetrically Laser-Scribed Reduced Graphene Oxide Paper Electrodes. *ACS Nano* **2014**, *8*, 2986–2997. [CrossRef] [PubMed]
58. Wang, Y.; Niu, Z.; Chen, J.; Zhai, Y.; Xu, Y.; Luo, S. Freestanding laser induced graphene paper based liquid sensors. *Carbon* **2019**, *153*, 472–480. [CrossRef]
59. Tian, H.; Shu, Y.; Cui, Y.-L.; Mi, W.-T.; Yang, Y.; Xie, D.; Ren, T.-L. Scalable fabrication of high-performance and flexible graphene strain sensors. *Nanoscale* **2014**, *6*, 699–705. [CrossRef]
60. Rahimi, R.; Ochoa, M.; Yu, W.; Ziaie, B. Highly Stretchable and Sensitive Unidirectional Strain Sensor via Laser Carbonization. *ACS Appl. Mater. Interfaces* **2015**, *7*, 4463–4470. [CrossRef]
61. Jeong, S.-Y.; Lee, J.-U.; Hong, S.-M.; Lee, C.-W.; Hwang, S.-H.; Cho, S.-C.; Shin, B.-S. Highly Skin-Conformal Laser-Induced Graphene-Based Human Motion Monitoring Sensor. *Nanomaterials* **2021**, *11*, 951. [CrossRef]
62. Groo, L.; Nasser, J.; Inman, D.J.; Sodano, H.A. Transfer printed laser induced graphene strain gauges for embedded sensing in fiberglass composites. *Compos. Part B: Eng.* **2021**, *219*, 108932. [CrossRef]

63. Carvalho, A.F.; Fernandes, A.J.S.; Leitão, C.; Deuermeier, J.; Marques, A.C.; Martins, R.; Fortunato, E.; Costa, F.M. Laser-Induced Graphene Strain Sensors Produced by Ultraviolet Irradiation of Polyimide. *Adv. Funct. Mater.* **2018**, *28*, 1805271. [CrossRef]
64. Sun, B.; McCay, R.N.; Goswami, S.; Xu, Y.; Zhang, C.; Ling, Y.; Lin, J.; Yan, Z. Gas-Permeable, Multifunctional On-Skin Electronics Based on Laser-Induced Porous Graphene and Sugar-Templated Elastomer Sponges. *Adv. Mater.* **2018**, *30*, 1804327. [CrossRef] [PubMed]
65. Tao, L.-Q.; Tian, H.; Liu, Y.; Ju, Z.-Y.; Pang, Y.; Chen, Y.-Q.; Wang, D.-Y.; Tian, X.-G.; Yan, J.-C.; Deng, N.-Q.; et al. An intelligent artificial throat with sound-sensing ability based on laser induced graphene. *Nat. Commun.* **2017**, *8*, 14579. [CrossRef]
66. Cheng, C.; Wang, S.; Wu, J.; Yu, Y.; Li, R.; Eda, S.; Chen, J.; Feng, G.; Lawrie, B.; Hu, A. Bisphenol A Sensors on Polyimide Fabricated by Laser Direct Writing for Onsite River Water Monitoring at Attomolar Concentration. *ACS Appl. Mater. Interfaces* **2016**, *8*, 17784–17792. [CrossRef] [PubMed]
67. Nayak, P.; Kurra, N.; Xia, C.; Alshareef, H.N. Highly Efficient Laser Scribed Graphene Electrodes for On-Chip Electrochemical Sensing Applications. *Adv. Electron. Mater.* **2016**, *2*, 1600185. [CrossRef]
68. Fenzl, C.; Nayak, P.; Hirsch, T.; Wolfbeis, O.S.; Alshareef, H.N.; Baeumner, A.J. Laser-Scribed Graphene Electrodes for Aptamer-Based Biosensing. *ACS Sens.* **2017**, *2*, 616–620. [CrossRef]
69. Santos, N.F.; Pereira, S.O.; Moreira, A.; Girão, A.V.; Carvalho, A.F.; Fernandes, A.J.S.; Costa, F.M. IR and UV Laser-Induced Graphene: Application as Dopamine Electrochemical Sensors. *Adv. Mater. Technol.* **2021**, *6*, 2100007. [CrossRef]
70. Vanegas, D.C.; Patiño, L.; Mendez, C.; Oliveira, D.A.; Torres, A.M.; Gomes, C.L.; McLamore, E.S. Laser Scribed Graphene Biosensor for Detection of Biogenic Amines in Food Samples Using Locally Sourced Materials. *Biosensors* **2018**, *8*. [CrossRef]
71. Soares, R.R.A.; Hjort, R.G.; Pola, C.C.; Parate, K.; Reis, E.L.; Soares, N.F.F.; McLamore, E.S.; Claussen, J.C.; Gomes, C.L. Laser-Induced Graphene Electrochemical Immunosensors for Rapid and Label-Free Monitoring of Salmonella enterica in Chicken Broth. *ACS Sens.* **2020**, *5*, 1900–1911. [CrossRef]
72. Marques, A.C.; Cardoso, A.R.; Martins, R.; Sales, M.G.F.; Fortunato, E. Laser-Induced Graphene-Based Platforms for Dual Biorecognition of Molecules. *ACS Appl. Nano Mater.* **2020**, *3*, 2795–2803. [CrossRef]
73. Kazemzadeh, R.; Andersen, K.; Motha, L.; Kim, W.S. Highly Sensitive Pressure Sensor Array With Photothermally Reduced Graphene Oxide. *IEEE Electron Device Lett.* **2015**, *36*, 180–182. [CrossRef]
74. Kazemzadeh, R.; Woo Soo, K. Flexible Temperature Sensor with Laser Scribed Graphene Oxide. In Proceedings of the 14th IEEE International Conference on Nanotechnology, Bangkok, Thailand, 18–21 August 2014; pp. 420–423.
75. Gholami Laelabadi, K.; Moradian, R.; Manouchehri, I. One-Step Fabrication of Flexible, Cost/Time Effective, and High Energy Storage Reduced Graphene Oxide@PANI Supercapacitor. *ACS Appl. Energy Mater.* **2020**, *3*, 5301–5312. [CrossRef]
76. Yu, X.; Li, N.; Zhang, S.; Liu, C.; Chen, L.; Han, S.; Song, Y.; Han, M.; Wang, Z. Ultra-thick 3D graphene frameworks with hierarchical pores for high-performance flexible micro-supercapacitors. *J. Power Sources* **2020**, *478*, 229075. [CrossRef]
77. Cai, F.; Tao, C.-A.; Li, Y.; Yin, W.; Wang, X.; Wang, J. Effects of amount of graphene oxide and the times of LightScribe on the performance of all-solid-state flexible graphene-based micro-supercapacitors. *Mater. Res. Express* **2017**, *4*, 036304. [CrossRef]
78. Gao, W.; Singh, N.; Song, L.; Liu, Z.; Reddy, A.L.M.; Ci, L.; Vajtai, R.; Zhang, Q.; Wei, B.; Ajayan, P.M. Direct laser writing of micro-supercapacitors on hydrated graphite oxide films. *Nat. Nanotechnol.* **2011**, *6*, 496–500. [CrossRef] [PubMed]
79. Liu, H.; Moon, K.-S.; Li, J.; Xie, Y.; Liu, J.; Sun, Z.; Lu, L.; Tang, Y.; Wong, C.-P. Laser-oxidized Fe3O4 nanoparticles anchored on 3D macroporous graphene flexible electrodes for ultrahigh-energy in-plane hybrid micro-supercapacitors. *Nano Energy* **2020**, *77*, 105058. [CrossRef]
80. Peng, Z.; Lin, J.; Ye, R.; Samuel, E.L.G.; Tour, J.M. Flexible and Stackable Laser-Induced Graphene Supercapacitors. *ACS Appl. Mater. Interfaces* **2015**, *7*, 3414–3419. [CrossRef]
81. Peng, Z.; Ye, R.; Mann, J.A.; Zakhidov, D.; Li, Y.; Smalley, P.R.; Lin, J.; Tour, J.M. Flexible Boron-Doped Laser-Induced Graphene Microsupercapacitors. *ACS Nano* **2015**, *9*, 5868–5875. [CrossRef]
82. Song, W.X.; Zhu, J.X.; Gan, B.H.; Zhao, S.Y.; Wang, H.; Li, C.J.; Wang, J. Flexible, Stretchable, and Transparent Planar Microsupercapacitors Based on 3D Porous Laser-Induced Graphene. *Small* **2018**, *14*, 1702249. [CrossRef]
83. Steele, B.C.H.; Heinzel, A. Materials for fuel-cell technologies. *Nature* **2001**, *414*, 345–352. [CrossRef] [PubMed]
84. Tee, S.Y.; Win, K.Y.; Teo, W.S.; Koh, L.-D.; Liu, S.; Teng, C.P.; Han, M.-Y. Recent Progress in Energy-Driven Water Splitting. *Adv. Sci.* **2017**, *4*, 1600337. [CrossRef] [PubMed]
85. Li, Y.; Sun, Y.; Qin, Y.; Zhang, W.; Wang, L.; Luo, M.; Yang, H.; Guo, S. Recent Advances on Water-Splitting Electrocatalysis Mediated by Noble-Metal-Based Nanostructured Materials. *Adv. Energy Mater.* **2020**, *10*, 1903120. [CrossRef]
86. Zhang, J.; Ren, M.; Wang, L.; Li, Y.; Yakobson, B.I.; Tour, J.M. Oxidized Laser-Induced Graphene for Efficient Oxygen Electrocatalysis. *Adv. Mater.* **2018**, *30*, 1707319. [CrossRef] [PubMed]
87. Hu, W.; Peng, C.; Luo, W.; Lv, M.; Li, X.; Li, D.; Huang, Q.; Fan, C. Graphene-Based Antibacterial Paper. *ACS Nano* **2010**, *4*, 4317–4323. [CrossRef]
88. Singh, S.P.; Li, Y.; Be'er, A.; Oren, Y.; Tour, J.M.; Arnusch, C.J. Laser-Induced Graphene Layers and Electrodes Prevents Microbial Fouling and Exerts Antimicrobial Action. *ACS Appl. Mater. Interfaces* **2017**, *9*, 18238–18247. [CrossRef]
89. Stanford, M.G.; Li, J.T.; Chen, Y.; McHugh, E.A.; Liopo, A.; Xiao, H.; Tour, J.M. Self-Sterilizing Laser-Induced Graphene Bacterial Air Filter. *ACS Nano* **2019**, *13*, 11912–11920. [CrossRef]
90. Rathinam, K.; Singh, S.P.; Li, Y.; Kasher, R.; Tour, J.M.; Arnusch, C.J. Polyimide derived laser-induced graphene as adsorbent for cationic and anionic dyes. *Carbon* **2017**, *124*, 515–524. [CrossRef]